The following publication C. C. T. Chow, M. Zhang and K. T. Chau, "Analytical AC Loss Comparison Between REBCO, MgB_2, Copper, and Aluminum Litz Wires for Cryogenic Electrical Machines," in IEEE Transactions on Applied Superconductivity, vol. 35, no. 2, pp. 1-16, March 2025, Art no. 5201416 is available at https://doi.org/10.1109/tasc.2024.3519419.

Analytical ac loss comparison between REBCO, MgB_2, copper and aluminum Litz wires for cryogenic electrical machines

Calvin C. T. Chow, *Graduate Student Member, IEEE* Min Zhang, *Senior Member, IEEE* and K. T. Chau *Fellow, IEEE*

***Abstract*—Cryogenic electrical machines can have high power densities because conductors can carry large current densities at low temperatures. This paper compares four types of conductors: copper Litz wire, aluminum Litz wire, MgB_2 multifilamentary wire, and REBCO tape, and one set of material parameters are used for each conductor for case studies in this paper. Based on analytical loss formulas from the literature, the conductors' loss at different engineering current densities, temperatures and external magnetic fields are compared. The effect of striating REBCO tapes is also investigated. On an individual conductor level, under simultaneous transport ac with external ac field of amplitude 0.4 T, both at 150 Hz, we find that when MgB_2 and REBCO carry ac close to their critical current densities, their losses are lower than the losses of the Litz wires at the same current densities. Further, we consider 3 MW, 4,500 rpm, 150 Hz machines with magnetic loading of 0.4 T when the armature is made of the different conductors. As the current density in armature conductors increases, the machine volume decreases. At 77.5 K, machines with copper and aluminum Litz wires have lower losses than machines with REBCO for the same machine volumes. At 20 K, for small machine volumes, machines with aluminum Litz wire armatures have the lowest losses.**

***Index Terms*—Superconducting machines, REBCO, MgB_2, Litz wire, ac loss, T-A homogenized formulation**

I. Introduction

Electrical machines with high power densities (kW/kg) can be useful in many applications, for example, in electric motors for aircraft or in wind turbine generators, both of which have received significant interest as the world seeks to reduce its carbon emissions.

There are numerous ways to increase the power density of electrical machines, for example, by using conductors with high current densities. In future, in a hydrogen economy, electric aircraft may use hydrogen as fuel, and thus the free cooling power can be exploited. Cooling copper or aluminum to cryogenic temperatures can reduce their resistivities and thus increase their current densities; on the other hand, superconductors can carry very high current densities, but suffer from problems such as the possibility of quench and cost.

Two superconductors, namely, MgB_2 and REBCO (where "RE" is a rare-earth element, for example, Y or Gd), are of interest. MgB_2 has low cost compared to REBCO and can be made into fine filaments and this helps reduce ac loss. Reducing ac loss is important when superconductors are used in the stator of a machine, where time-varying magnetic field is experienced whilst transport ac is carried in the conductors. REBCO is also popular due to its high critical current density.

The H2GEAR project, led by GKN Aerospace, is developing a powertrain for future hydrogen-powered aircraft that accommodates up to 96 passengers using cryogenic normal-state conductor rather than using superconductor, citing the reason that using more conventional materials makes the system deliverable sooner [1]. However, superconductors may be the only candidate that is able to deliver a light enough powertrain for large aircraft, and the ASuMED [2] and ASCEND [3] projects investigated superconducting motor and powertrain, respectively. Following ASCEND, Airbus is now developing a 2 MW superconducting electric propulsion system demonstrator in the new project called Cryoprop.

Sumption [4] compared the losses of YBCO and MgB_2 under specific conditions, and Sumption et al. [5] provided maximum current densities (according to different criteria) for different materials including copper, aluminum, MgB_2 and REBCO operating under transport dc, as well as simultaneous transport ac and alternating external magnetic field. Expected reduction in mass and volume of machines when the machines were made of different materials were also provided. However, only specific temperatures and fields were considered. Thus, this paper extends the loss calculations to other temperatures and fields. Haugan et al. [6] compared the mass and loss of an aircraft electrical distribution system when cables were made of copper-cladded aluminum, hyperconducting aluminum and YBCO. On a machine level, Kalsi et al. [7] compared two machines whose armatures were made of REBCO CORC cables and MgB_2 (both at 20 K), respectively, and it was found that the former had higher power density (excluding cooler) but also higher loss. Nam et al. [8] compared wind

This work was supported in part by the Hong Kong Research Grants Council under Project No. 17204021, and The Hong Kong Polytechnic University under Project Nos. P0048560 and P0046563, Hong Kong Special Administrative Region, China. Most of this paper forms part of the Ph.D. dissertation of Calvin C. T. Chow. *(Corresponding author: k.t.chau@polyu.edu.hk)*

Calvin C. T. Chow was with Department of Electronics and Electrical Engineering, University of Strathclyde, G1 1XQ Glasgow, U.K., on leave from the Department of Electrical and Electronic Engineering, University of Hong Kong, Pokfulam, Hong Kong SAR, China. He is now with the Research Centre for Electric Vehicles and Department of Electrical and Electronic Engineering, The Hong Kong Polytechnic University, Hung Hom, Kowloon, Hong Kong SAR, China.

Min Zhang is with the Department of Electronics and Electrical Engineering, University of Strathclyde, G1 1XQ Glasgow, United Kingdom.

K. T. Chau is with the Research Centre for Electric Vehicles and Department of Electrical and Electronic Engineering, The Hong Kong Polytechnic University, Hung Hom, Kowloon, Hong Kong SAR, China.

generators made of YBCO and MgB_2 field coils and found that the former was lighter and smaller.

This paper compares the performance of copper and aluminum Litz wires, MgB_2 and REBCO on an isolated conductor level, and when they are used in the armatures of electrical machines. In particular, the loss values are compared, since the current that can flow in conductors are limited by the amount of heat that can be tolerated by the cooling system. Analytical formulas and critical current datasets are taken from the literature for the purpose of loss calculations. In contrast to much of literature, comparisons on an isolated-conductor level are made for a continuous range of temperatures (20 K to 270 K), fields and transport current values, rather than at discrete values, and thus allowing trends to be seen as a variable changes. Further, a machine sizing formula is used to estimate the diameter of a machine when different current densities flow in the stator conductors. A simple machine design procedure is provided to design air-cored machines with different armature and rotor current densities to output a rated power of 3 MW; numerical simulations are performed to verify the output torque predicted by the machine sizing formula. In addition, loss in the armature is estimated based on largely analytical formulas. For REBCO in armature slots, formulas by Clem et al. [9] are used to calculate transport ac loss of a finite stack of tapes, and taking inspiration from Yuan et al. [10], we modify [9] to calculate magnetization loss too for a finite stack of tapes. Comparison between analytical formulas and numerical simulations are provided for loss in machines with REBCO armatures. In the numerical simulations, the homogenized T-A formulation is used to simulate stacks of REBCO tapes in a slot in the armature. The volumes and the losses of 3 MW machines with armatures made of the four different conductors with different current densities are estimated.

The rest of the paper is organized as follows. Section II gives the geometry of the conductors and the formulas used to estimate losses for isolated conductors. Section III gives formulas to estimate transport ac loss and magnetization loss in a stack of REBCO tapes. Section IV compares the conductors on an isolated conductor level when each conductor is simultaneously carrying transport ac and subject to an alternating external magnetic field. Section V compares the volumes and losses of machines whose armatures are made of the different conductors. Finally, Section VI states the limitations of this study and we conclude in Section VII.

II. Loss formulas for different materials in isolation

A. Copper and aluminum Litz wires

For a Litz wire made of cylindrical filaments with a linear magnetic material, provided the filament diameter is less than the skin depth δ, the loss per unit length (W/m) when it is subject to a sinusoidally varying external magentic field of amplitude $\hat{H}$ and carrying sinusoidally varying transport ac of amplitude $\hat{I}$, both at frequency f, is [11]

TABLE I: Parameters of Copper and Aluminum Litz Wires

Description	Symbol	Unit	Value
Number of filaments in wire	N	-	270
Radius of a filament	r_s	mm	0.04
Radius of Litz wire	r_L	mm	0.95

Data from supplier [12]. The filament diameter corresponds to AWG 40, which was a diameter used in [5], and was also used in motor design and statorette experiment in [13]. A slotless high-frequency permanent magnet synchronous machine [14], [15] used AWG 38, which is only slightly larger. The Litz wire diameter is the mean of the maximum and minimum outer diameter of the Grade 1 unserved Litz wire provided in [12].

TABLE II: Coefficients for Resistivity Formula (2)

Coefficient	Value for copper	Value for aluminum
a_0	3.692×10^{-1}	-7.55×10^{-2}
a_1	2.214×10^{-3}	2.167×10^{-2}
a_2	-4.312×10^{-4}	-1.283×10^{-3}
a_3	1.679×10^{-5}	2.836×10^{-5}
a_4	-9.311×10^{-8}	-1.306×10^{-7}
b_0	-2.484	-1.944
b_1	5.699×10^{-2}	1.958×10^{-3}
b_2	1.078×10^{-4}	9.07×10^{-4}
b_3	-3.917×10^{-7}	-2.959×10^{-6}
b_4	4.405×10^{-10}	3.447×10^{-9}

$$P_{\text{Litz}} = \frac{R_{\text{dc}}\hat{I}^2}{2} + \frac{R_{\text{dc}}\hat{I}^2}{2}\left(\frac{N(N-1)}{8}\left(\frac{r_s}{r_L}\right)^2\left(\frac{r_s}{\delta}\right)^4\right) + \frac{N}{8}\omega^2(\mu\hat{H})^2\sigma\pi r_s^4 \tag{1a}$$

$$R_{\text{dc}} = \frac{1}{N\sigma\pi r_s^2} \tag{1b}$$

$$\delta = \sqrt{\frac{2}{\omega\mu\sigma}}, \tag{1c}$$

where μ is taken as the permeability of free space μ_0, $\omega = 2\pi f$ is the angular frequency, $\sigma = 1/\rho$ is the conductance and is the inverse of the resistivity of the filament material (copper or aluminum), and the rest of the parameters and their values are defined in Table I. The three terms in (1a) are the 'rms' loss, skin loss and proximity loss, respectively [11]. The resistivities of copper and aluminum at different temperatures are [11]:

$$\rho(T) = \begin{cases} a_0 + a_1T + a_2T^2 + a_3T^3 + a_4T^4, & 20 \le T \le T_x \\ b_0 + b_1T + b_2T^2 + b_3T^3 + b_4T^4, & T_x \le T \le 270 \end{cases} \tag{2}$$

where ρ is the resistivity in nΩ·m; T is the temperature in K; values of coefficients are given in Table II; T_x is 75.4 K and 75.1 K for copper and aluminum, respectively. For 300 K, we take the resistivities of copper and aluminum as 1.73 $\mu\Omega$cm and 2.72 $\mu\Omega$cm, respectively [5].

B. MgB_2

The geometry of the MgB_2 multifilamentary wire considered consists of MgB_2 filaments embedded in a matrix, which

is in turn surrounded by an outer sheath. There is a central area (called the core) in the matrix in which there is no filament and only the matrix material is present. Details of the geometry are given in Table III, which are mainly taken from the wire with strand code 3799 detailed in [16].

When the multifilamentary wire is subject to sinusoidally varying external field of amplitude $\hat{H}$ and carrying sinusoidally varying transport ac of amplitude $\hat{I}$, both at frequency f, the total average loss P_t (in W/m) can be estimated as [4], [5], [16][1]

$$P_t = P_h + P_e + P_c + P_I + P_x, \tag{3}$$

where P_h is the hysteresis loss in the superconducting filaments, P_e is the eddy current loss in metal outer sheath, P_c is the coupling loss in matrix and superconductor. P_h, P_e and P_c are due to the external magnetic field. P_I is the transport ac loss due to transport ac in the superconducting filaments. These are given as follows. P_x is the interaction term and will be ignored for simplicity [4].

For frequency less than $4\pi\rho_{\rm tf}/(\mu_0 L_p^2)$, assuming fully penetrated filaments and relatively long twist pitch ($L_p/(2\pi r_0) > 3$ [20, p.127]), the average hysteresis loss (in W/m) is [20, (9.56) multiplied by wire area]

$$P_h = \lambda f \frac{8}{3\pi} J_c d_{\rm fil} \mu_0 \hat{H} \pi r_0^2 \tag{4}$$

where $J_c = J_c(T, \mu_0\hat{H})$ is the critical current density of the filament.

The sum of eddy current loss and coupling loss per unit volume is given in [21, (3.10)], which when multiplied by the area of conductor and noting $1/T \int_0^T \dot{B}^2\, dt = 2(\pi f \hat{B})^2$ and taking $\hat{B} = \mu_0\hat{H}$, we get the sum of eddy current loss and coupling loss per unit length as

$$\begin{aligned} P_e + P_c =& 2(\pi f \mu_0 \hat{H})^2 \Bigg(\left(\frac{r_f}{r_0}\right)^2 \left(\frac{L_{\rm p,M}}{2\pi}\right)^2 \left(\frac{1}{\rho_{\rm ms}} \frac{r_0^2 - r_f^2}{r_0^2 + r_f^2} \right. \\ &\left. + \frac{1}{\rho_{\rm tf}} \frac{r_f^2 - r_c^2}{r_f^2} + \frac{1}{\rho_{\rm mc}} \frac{r_c^2}{r_f^2} \right) + \frac{r_0^4 - r_f^4}{4\rho_{\rm ms} r_0^2} \Bigg) \pi r_0^2. \end{aligned} \tag{5}$$

Finally, the average transport ac loss per unit length is [7]

$$P_I = \frac{\mu_0 f}{\pi} I_c^2 \left((1-\Gamma)\ln(1-\Gamma) + \Gamma - \frac{\Gamma^2}{2} \right). \tag{6}$$

where $\Gamma = \hat{I}/I_{c,\rm M}$ and $I_{c,\rm M} = J_{c,\rm M}\lambda\pi r_0^2$ is the critical current of multifilamentary wire.

The critical current of an MgB_2 wire is $I_{c,\rm M} = J_{c,\rm M}\lambda\pi r_0^2$, where the critical current density $J_{c,\rm M}(T,B)$ (in A/m^2) of MgB_2 filament at different temperature T (in K) and external magnetic field B (in T) has the form given in [22]

$$J_{c,\rm M}(T,B) = J_{c0}(t) \exp\left(-\frac{B^m}{B_0(t)}\right) \tag{7a}$$

$$J_{c0}(t) = J_{c00}(1-\alpha t^2) \tag{7b}$$

$$B_0(t) = B_{00}(1-\beta t), \tag{7c}$$

[1]This addition is a simple approximation. Such approach is also used for estimating loss in machines in [7], [17], [18]. However, comparison between similar theoretical analysis and experiments are done in [19], with good agreements found.

TABLE III: Parameters of Multifilamentary MgB_2 Wire

Description	Symbol	Unit	Value
Number of MgB_2 filaments	-	-	114 [16, Table 1]
Radius of core	r_c	μm	44 [16, Table 5]
Radius of matrix (inner radius of outer sheath)	r_f	μm	191 [16, Table 5]
Outer radius of outer sheath	r_0	μm	240 [16, Table 5]
Twist pitch	$L_{\rm p,M}$	mm	10
Diameter of an MgB_2 filament	$d_{\rm fil}$	μm	14.8 [16, Table 4]
Resistivity of core	$\rho_{\rm mc}$	nΩm	117 [16, Table 1]
Transverse resistivity of filamentary zone	$\rho_{\rm tf}$	nΩm	46 [16, Table 5]
Resistivity of outer sheath	$\rho_{\rm ms}$	nΩm	360 [16, Table 1]
Proportion of the composite wire occupied by MgB_2	λ	-	0.12 [16, Table 1]

Parameters are mainly taken from parameters of the wire with strand code 3799 detailed in [16].

TABLE IV: Parameters of REBCO Tape

Description	Symbol	Unit	Value
Number of REBCO filaments	$N_{\rm R}$	-	10
Width of multifilamentary tape	$w_{\rm tape}$	mm	4
Width of a groove	$w_{\rm grv}$	μm	20 [23]
Thickness of upper copper layer	$t_{\rm Cu1}$	μm	5 [24]
Thickness of upper silver layer	$t_{\rm Ag1}$	μm	2 [24]
Thickness of REBCO layer	$t_{\rm R}$	μm	2.35 [24]
Thickness of substrate	$t_{\rm H}$	μm	40 [24]
Thickness of lower silver layer	$t_{\rm Ag2}$	μm	1 [24]
Thickness of lower copper layer	$t_{\rm Cu2}$	μm	5 [24]
Thickness of whole tape	$t_{\rm tape}$	μm	55.65
Twist pitch	$L_{\rm p,R}$	m	0.3
Resistivity of Hastelloy substrate	$\rho_{\rm H}$	μΩm	1.23 [25]
Resistivity of copper	$\rho_{\rm Cu}$	nΩm	(2)
Resistivity of silver	$\rho_{\rm Ag}$	Ωm	interpolation of [26, p.1260]

where, in this paper, we take $t = T/35.2$, $\alpha = 1.1$, $\beta = 1$, $J_{c00} = 10^6$ A cm^{-2}, $B_{00} = 4$, and $m = 1.2$. When the MgB_2 composite wire is under an alternating external magnetic field, the $J_{c,\rm M}(T,B)$ of MgB_2 filaments is calculated in this paper with B being the amplitude of the alternating external magnetic field.

C. REBCO

1) REBCO tape in isolation: REBCO is supplied in the form of a composite tape consisting of different layers, and the superconducting REBCO layer is only a thin layer in the composite tape. To reduce ac loss, the REBCO layer can be striated [27], [28] into $N_{\rm R}$ filaments. The total loss of such a tape subject to sinusoidally varying external field of amplitude $\hat{H}$ and carrying sinusoidally varying transport ac of amplitude $\hat{I}$, both at frequency f, is given by (3). P_h is the hysteresis loss in the superconducting material, P_e is the eddy current loss in metal layers, P_c is the coupling loss due to coupling current that runs through the superconducting material and metal. P_h, P_e and P_c are due to the external magnetic field. P_I is the transport ac loss due to transport ac in the superconducting

material. The terms in (3) are given as follows. Details of the geometry of the REBCO tape are given in Table IV, which contains variables used in the following equations. Many of the parameters are based on Molodyk et al. [24]. The layers in the tape, from top to bottom, are: upper copper layer (5 μm), upper silver layer (2 μm), REBCO (2.35 μm), buffer layers (≈ 0.3 μm), Hastelloy (40 μm), lower silver layer (1 μm), and lower copper layer (5 μm). The total thickness is thus 55.65 μm.

The hysteresis loss (in W/m) of a thin unstriated REBCO strip due to the external magnetic field is given by Brandt and Indenbom [29]

$$P_{h,\text{Brandt}} = \mu_0 w_{\text{strip}}^2 J_{\text{cs}} \hat{H} \left(\frac{2H_c}{\hat{H}} \ln\left(\cosh\left(\frac{\hat{H}}{H_c} \right) \right) - \tanh\left(\frac{\hat{H}}{H_c} \right) \right) f, \tag{8}$$

where w_{strip} is the width of the strip, $H_c = J_{\text{cs}}/\pi$, J_{cs} is the sheet critical current density (A/m) given by $J_{\text{cs}} = I_c/w_{\text{strip}}$ where I_c is the critical current of the REBCO strip.

For striated tapes, we approximate the hysteresis loss by a formula by Mawatari [30], which gives the hysteresis loss per cycle per unit volume of an infinite array of thin superconducting strips under perpendicular external magnetic field. Multiplying the formula of Mawatari [30] by the cross-sectional area of the filaments, we calculate the hysteresis loss per unit length of a striated REBCO tape as

$$P_h = -(f N_{\text{R}} w_{\text{fil}} t_{\text{R}}) \frac{2\mu_0 L_{\text{cell}}^2}{\pi w_{\text{fil,h}} t_{\text{R}}} \int_0^{\hat{H}} \mathrm{d}\xi (\hat{H} - 2\xi) \times \ln\left[1 - \frac{\sin^2(\pi w_{\text{fil,h}}/L_{\text{cell}})}{\cosh^2(\xi/H_c)} \right], \tag{9}$$

where $w_{\text{fil,h}} = w_{\text{fil}}/2$ is half the width of a filament, the width of a filament being $w_{\text{fil}} = (w_{\text{tape}} - w_{\text{grv}}(N_{\text{R}} - 1))/N_{\text{R}}$ where w_{grv} is the width of a groove. $H_c = J_{\text{cs}}/\pi$,J_{cs} is the sheet critical current density (A/m) given by $J_{\text{cs}} = I_c/(w_{\text{fil}} N_{\text{R}})$ where I_c is the critical current of the whole striated REBCO tape. L_{cell} is the width of a periodic unit cell of the infinite array in Mawatari's formula, and is taken as the sum of the filament width and groove width [28], $L_{\text{cell}} = w_{\text{fil}} + w_{\text{grv}}$. For simplicity, we use (9) regardless of the number of filaments, including the unstriated case, where $w_{\text{fil}} = w_{\text{tape}}$.

There are Hastelloy substrate, copper and silver layers in a REBCO tape, and eddy current loss is induced in these layers when the tape is subject to an external magnetic field. When the tape is striated, we assume the upper copper and upper silver layer are striated as well. The total eddy current loss is the sum of eddy current loss in the Hastelloy substrate, copper and silver layers. The eddy current loss in each metal layer i when acted on by an external magnetic field perpendicular to tape, provided metal layer's half-thickness ($t_i/2$) is less than the skin depth $\delta = \sqrt{\frac{\rho_i}{\pi f \mu_0}}$, is [31, (26)]

$$P_e = \frac{\pi^2}{6\rho_i} (\mu_0 \hat{H} w_i f)^2 t_i w_i N_i, \tag{10}$$

where t_i is the thickness of the layer i, i = Cu1, Cu2, Ag1, Ag2, H, denoting upper copper, lower copper, upper silver, lower silver, and Hastelloy layers, respectively; w_i is the width a filament w_{fil} if i = Cu1 and Ag1, and is the width of the tape w_{tape} if i = Cu2, Ag2 and H; N_i is the number of filaments N_{R} if i = Cu1 and Ag1, and is 1 if i = Cu2, Ag2 and H; ρ_i is the resistivity of layer i, where $\rho_{\text{Cu1}}, \rho_{\text{Cu2}}$ are given in (2), $\rho_{\text{Ag1}}, \rho_{\text{Ag2}}$ are calculated from interpolation of data by Matula [26, p.1260], and ρ_{H} is taken as temperature-independent as 1.23 μΩm, since the resistivity of Hastelloy is approximately 1.228-1.236 μΩm at in the range 20-80 K [25]. Equation (10) is the same as [32, (16)], which is for large field.

When a tape is striated by laser, the transverse resistivity is strongly affected by laser settings [33], which affect the resistivity and amount of redeposited material. Depending on the barrier resistance between superconductor and substrate, the path of the coupling current may be different [23], [33], [34], making it difficult to estimate the transverse resistance. For example, if transverse current flows predominately in the Hastelloy substrate instead of the barriers and the superconducting filaments, the equation for transverse resistivity by Oberly et al. [35, after (2)] cannot be used [33]. Carr et al. [36] suggested the transverse resistivity in the anisotropic continuum model can be written as

$$\rho_\perp = \frac{k t_{\text{R}}}{w_{\text{fil}}} \rho_{\text{H}}, \tag{11}$$

where w_{fil} is the width of a filament, t_{R} is the thickness of the superconducting layer, ρ_{H} is the resistivity of the Hastelloy substrate, and k is a parameter ranging from π to ∞ depending on the effect of the laser. The value of π is for the case when the resistance between the superconducting filaments and the substrate is zero, and the value of ∞ is when the laser removes the top silver layer, superconductor (and buffer) perfectly without redeposition resulting in complete filament decoupling [36]. The transverse resistivities of a 10-filament tape (SAE 5-μm) was experimentally measured by Godfrin et al. [23] to be approximately 10 nΩm. Taking the filament width w_{fil} to be 12 mm/10, thickness t_{R} to be 1.5 μm [23], $\rho_{\text{H}} = 1.23$ μΩm, applying (11), k is 6.5, which is towards the lower end of the range of k. In this paper, for simplicity, we assume $\rho_\perp$ to be temperature independent[2], and is given in (11) with $k = 6.5$.

The coupling loss (in W/m) for twisted multifilamentary strip conductor is [20, (12.23)]

$$P_c = \frac{1}{4\rho_\perp} (f L_{\text{p,R}} \mu_0 \hat{H})^2 w_{\text{tape}} t_{\text{R}}. \tag{12}$$

Finally, the average transport ac loss per unit length of the multifilamentary tape is [20, p.192]

$$P_I = \frac{\mu_0 f}{\pi} I_c^2 \left((1-\Gamma)\ln(1-\Gamma) + (1+\Gamma)\ln(1+\Gamma) - \Gamma^2 \right) \tag{13}$$

where $\Gamma = \hat{I}/I_{c,\text{R}}$ and $I_{c,\text{R}}$ is the critical current of the multifilamentary tape.

The critical current $I_{c,\text{R}}(T, B, N_{\text{R}})$ (in A) at different temperature T (in K) and external magnetic field B (in T) is obtained by interpolation of per cm width critical current

[2]Measurements of transverse resistivity of samples done above around 70 K in [37] were temperature independent.

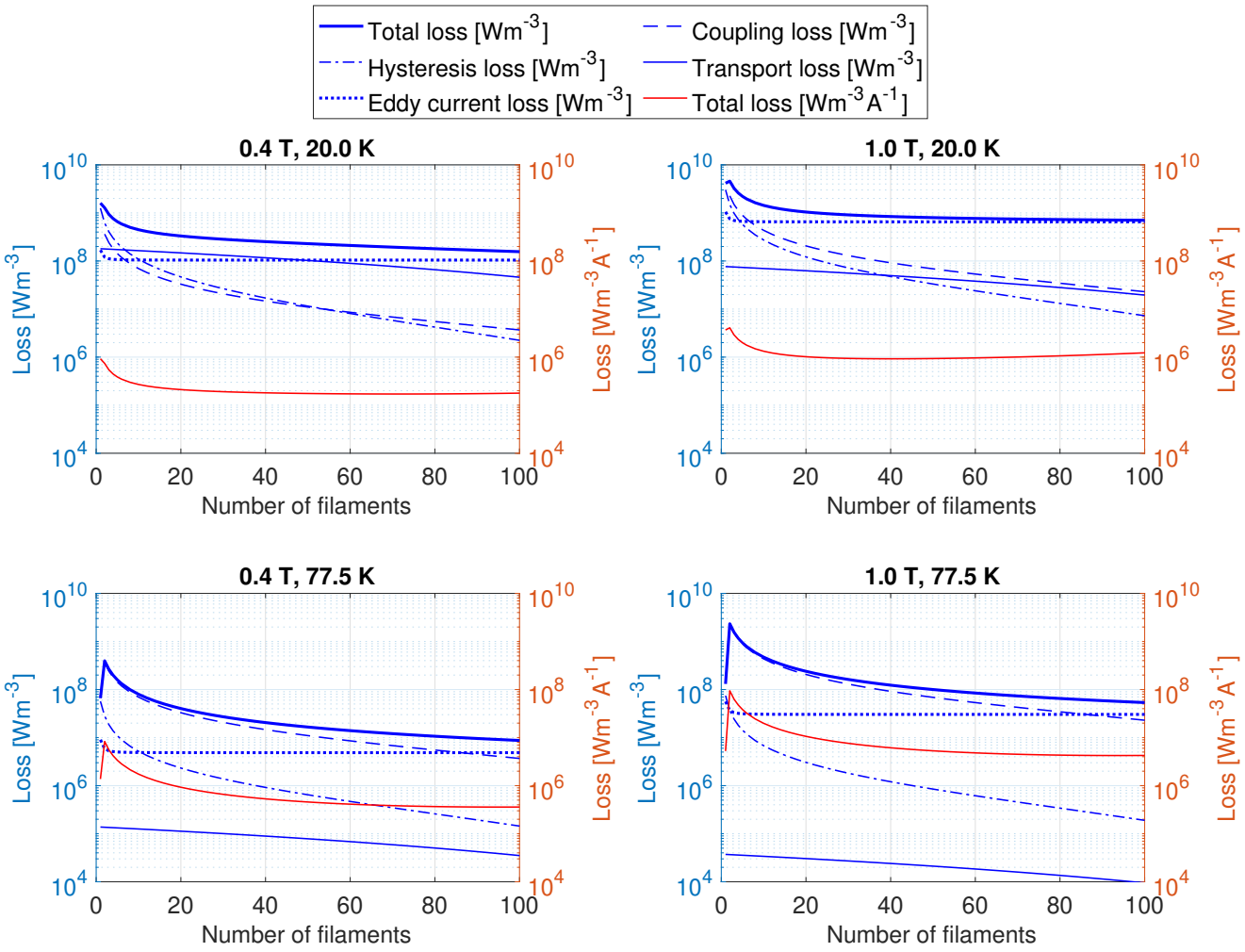

Fig. 1: Loss components in a REBCO tape when it is striated into different number of filaments. Performance at $T = 20$ K and 77.5 K are plotted. The tape carries 150 Hz transport ac with amplitude $0.9I_c(T, \hat{B}, N_\mathrm{R})$, whilst being under a 150 Hz alternating external magnetic field of amplitudes $\hat{B}$ of 0.4 T and 1 T, respectively.

$I_c(T, B)$ data of a SuperOx YBCO tape (at zero degree field angle) available on [38], multiplied by total width of all filaments. The additional reduction of critical current due to reasons other than the loss of REBCO material, which is equal to the sum of width of grooves, is not considered for simplicity. When the REBCO tape is under an alternating external magnetic field, its $I_{c,\mathrm{R}}(T, B)$ is calculated in this paper with B being the amplitude of the alternating external magnetic field.

2) Effect of striation on losses: To investigate the effectiveness of striation on reduction of ac loss, we plot in the left axes in Fig. 1 the loss per unit volume (loss per unit length divided by area of tape $w_\mathrm{tape} t_\mathrm{tape}$) of a REBCO tape with different number of filaments carrying a 150 Hz transport ac of amplitude $0.9I_c(T, B, N_\mathrm{R})$ whilst being under a 150 Hz alternating external magnetic field with amplitudes 0.4 T and 1 T, respectively. It can be seen that eddy current loss in the metal layers dominates at higher number of striation, thus, the effect of striation saturates at high number of striation. Also, for tapes at 77.5 K, striating the tapes can increase the total loss because of the coupling loss. Although the total loss of the tapes at 20 K is higher than at 77.5 K, the transport current carried at 20 K is also higher than that at 77.5 K: for N_R = 1–100, $0.9I_c(T = 20, B = 0.4, N_\mathrm{R})$ corresponds to 1740–886 A , and $0.9I_c(T = 77.5, B = 0.4, N_\mathrm{R})$ corresponds to 48–25 A; $0.9I_c(T = 20, B = 1, N_\mathrm{R})$ corresponds to 1130–577 A, and $0.9I_c(T = 77.5, B = 1, N_\mathrm{R})$ corresponds to 25–13 A. The tapes carry 90% of critical current, which changes with number of striation. Thus, we also plot on the right axes in Fig. 1 the total loss per unit volume per unit current amplitude. Compared to unstriated tapes, striating tapes to 100 filaments can reduce the total loss per unit volume per unit current in 0.4 T (by 74% at 77.5 K and 81% at 20 K) and in 1 T (by 19% at 77.5 K and 67% at 20 K). In design, the benefit of reduced hysteresis loss has to be balanced against the reduction in critical current (due to loss of REBCO material) and the presence of coupling loss.

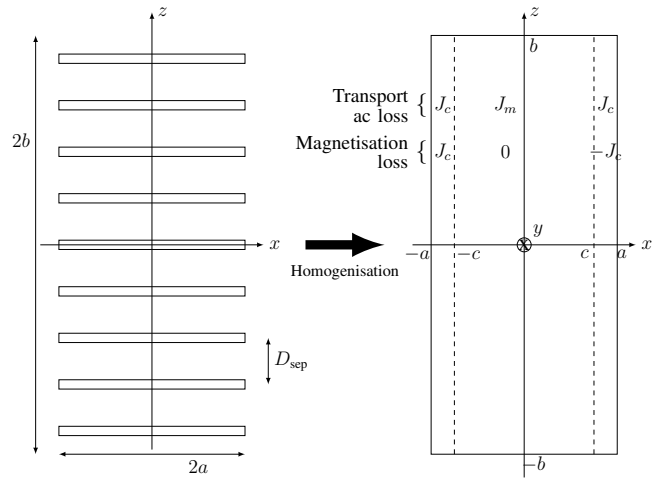

Fig. 2: The stack of tapes modeled and the homogenized bulk. The current density distribution when calculating transport ac loss and magnetization loss are also shown on the figure on the right.

III. Loss of REBCO tapes in a stack

A. Transport ac loss

For an infinitely thick stack of HTS tapes, equations to calculate the magnetization loss and transport ac loss are readily available [30], [39]–[41]. However, HTS coils are made of a finite number of tapes, so equations for a finite stack are needed. Clem et al. [9] provided simple equations to estimate transport ac loss of a stack of HTS tapes with finite stack height. The stack was modeled as an anisotropic bulk. The method is summarized as follows.

Consider a stack of HTS tapes extending infinitely long into the page in the y direction. The cross-section of the stack is on the x-z plane. The tapes have width $2a$ in the x direction; and the tapes are stacked in the z direction with distance D_{sep} between adjacent tapes, and the total stack height is $2b$. The thickness of each tape in z direction is d. Each tape has a critical current I_c and carries a transport current I. The stack is modeled as an anisotropic bulk, as shown in Fig. 2. The critical current density of the bulk $J_c = I_c/(2aD_{\text{sep}})$.

The current distribution in the bulk is separated into the critical and subcritical regions,

$$J_y = \begin{cases} J_c, & c < |x| < a \\ J_m & -c < x < c \end{cases}, \tag{14}$$

where

$$\frac{J_m}{J_c} = 1 - \frac{a}{c}\left(1 - \frac{I}{I_c}\right). \tag{15}$$

Since $0 < J_m < J_c$, c/a ranges from $1 - (I/I_c)$ to 1.

For better accuracy, $c = c(z), J_m = J_m(z)$ should be used, but for ease of calculation, Clem et al. [9] assumed c to be a constant. To find c, the following equation is solved numerically. In this paper, we minimize the absolute value of the left-hand-side of the following equation (specifically, the expression involving A_y), via the golden section search method, with c's starting range being $(1 - (I/I_c))a$ to a).

$$\int_0^b \int_0^c B_z(x,z)\,dx\,dz = \int_0^b A_y(c,z) - A_y(0,z)\,dz = 0, \tag{16}$$

where

$$A_y(x,z) = a^2\Big(f_y(-1,-c',b',x',z') + j_m f_y(-c',c',b',x',z') + f_y(c',1,b',x',z')\Big) \tag{17}$$

$$B_z(x,z) = a\Big(f_z(-1,-c',b',x',z') + j_m f_z(-c',c',b',x',z') + f_z(c',1,b',x',z')\Big) \tag{18}$$

$$f_y(x_1,x_2,b,x,z) = -\frac{\mu_0 J_c}{4\pi}\Bigg[\Bigg[uv\ln\left(u^2+v^2\right) + u^2\tan^{-1}\left(\frac{v}{u}\right) + v^2\tan^{-1}\left(\frac{u}{v}\right)\Bigg]_{u=x-x_1}^{x-x_2}\Bigg]_{v=z+b}^{z-b} \tag{19}$$

$$f_z(x_1,x_2,b,x,z) = -\frac{\mu_0 J_c}{2\pi}\Bigg[\Bigg[\frac{1}{2}v\ln\left(u^2+v^2\right) + u\tan^{-1}\left(\frac{v}{u}\right)\Bigg]_{u=x-x_1}^{x-x_2}\Bigg]_{v=z+b}^{z-b}. \tag{20}$$

where $j_m = 1 - \frac{a}{c}\left(1 - \frac{I}{I_c}\right), x' = x/a, z' = z/a, b' = b/a, c' = c/a$. $f_z(x_1,x_2,b,x,z)$ is the z component of $\mathbf{B}$ generated at (x,z) due to uniform current density J_c in region $x_1 < x < x_2$, $-b < z < b$. The resulting B_z is negative of what is presented in [9].

Once c is found, the transport ac loss Q' (in J/cycle/meter) of the bulk is

$$Q'_{\text{transp}} = 4Q'_{\text{init}} \tag{21}$$

$$Q'_{\text{init}} = -4J_c\int_0^b\int_c^a (a-x)B_z(x,z)\,dx\,dz. \tag{22}$$

To verify the method above numerically, the ac loss of a stack of tapes with different transport ac amplitudes is evaluated. The stack is made of tapes of width $2a = 12$ mm, $D_{\text{sep}} = 111.3$ μm, and stack height $2b = 8a$. Each tape has $I_c = 3,720$ A, and carries ac of varying amplitudes at 150 Hz. The above method, called semi-analytical method due to use of numerical procedures to find c in (16) and integration in (22), is used to evaluate the transport ac loss of the bulk. For comparison, the transport ac loss of the bulk is also calculated by T-A homogenized method [42] in COMSOL[3]. In addition, for reference, the result obtained by multiplying the loss of an isolated tape carrying transport ac of amplitude $\hat{I}$ by the

[3]In COMSOL simulations, the E-J power law is used, with $n = 30$, $E_c = 1 \times 10^{-4}$ V/m, $J_c = 1.32 \times 10^{11}$ A/m^2 of the HTS layer in a tape; HTS layer thickness is 2.35 μm. Current imposed on each tape is $\hat{I}\cos(2\pi ft - 2\pi/3)r(t)$ where the ramp function $r(t) = 1/(1+\exp(-5(10ft-1.8)))$, f = 150 Hz, and $\hat{I}$ is the current amplitude. One period is simulated, and the average transport ac loss is calculated by averaging the loss in the second half of the period simulated.

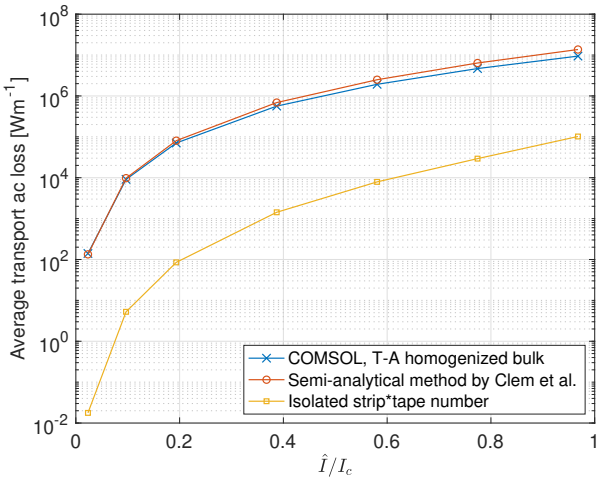

Fig. 3: Transport ac loss of a stack of tapes calculated by the semi-analytical method by Clem et al. [9], T-A homogenized method in COMOSL, and Norris formula for an isolated strip. Each 12 mm wide tape has $I_c = 3,720$ A. Stack height $2b = 48$ mm. Tape separation $D_{\text{sep}} = 111.3$ µm.

number of tapes is also plotted. The average power loss (W/m) of an isolated thin strip carrying transport ac is [43] (same as (13))

$$P = \frac{\mu_0 I_c^2 f}{\pi}\left((1-\Gamma)\ln(1-\Gamma) + (1+\Gamma)\ln(1+\Gamma) - \Gamma^2\right), \tag{23}$$

where $\Gamma = I/I_c$.

The results are shown in Fig. 3. There is some discrepancy between COMSOL and the method by Clem et al. at higher values of $\hat{I}/I_c$ (discrepancy of 31% at $\hat{I}/I_c = 0.967$). This is possibly due to the restriction of assuming constant c rather than allowing $c(z)$ to vary with z. This accuracy may be deemed acceptable at the initial design stages of a machine, and higher accuracy can be obtained by numerical simulation. However, simply multiplying the loss of an isolated tape by the number of tapes present in the stack gives results that are orders of magnitude smaller than the method by Clem et al., thus showing the importance of considering the tapes together as a stack when calculating ac loss.

B. Magnetization loss

Yuan et al. [10] modified the method by Clem et al. [9] by allowing $c(z)$, and extended it to the situation of alternating magnetic field in the z direction. To calculate the loss of a stack of tapes (modeled as a bulk) under alternating magnetic field of amplitude $\hat{B}_a$, this paper modifies [9] in light of [10], as follows. With reference from [10, eq. (9)], the current distribution in the bulk magnetized by a magnetic field $\hat{B}_a$ is

$$J_y = \begin{cases} -J_c, & c < x < a \\ 0 & -c < x < c \\ J_c, & -a < x < -c \end{cases}. \tag{24}$$

Taking into account the external field $\hat{B}_a$ and noting there is no current for $-c < x < c$,

$$B_z(x,z) = \hat{B}_a + a\Big(f_z(-1,-c',b',x',z') - f_z(c',1,b',x',z')\Big). \tag{25}$$

We continue to use constant c, which is found by solving the following numerically (via the golden section method in this paper),

$$\int_0^b \int_0^c B_z(x,z)\,dx\,dz = 0. \tag{26}$$

Once c is found, the magnetization loss Q' (in J/cycle/meter) of the bulk is

$$Q'_{\text{mag}} = 4Q'_{\text{init, mag}} \tag{27}$$

$$Q'_{\text{init, mag}} = 4J_c \int_0^b \int_c^a (a-x)B_z(x,z)\,dx\,dz. \tag{28}$$

To verify the above procedure, we calculate the magnetization loss of a stack of tapes made of tapes of width $2a = 4$ mm, stack height $2b = 0.01964$ m, made of tapes with $I_c = 1927$ A each and tape separation 111.6 µm (176 tapes in stack). The bulk is subject to alternating magnetic field in the z direction of various amplitudes $\hat{B}_a$, at $f = 150$ Hz. The above modified Clem procedure is used to evaluate the magnetization loss. Further, the magnetization of the bulk is also evaluated in COMSOL using T-A homogenized method [4]. In addition, for reference, the result obtained by multiplying the loss of an isolated tape under alternating magnetic field (perpendicular to tapes' face) of amplitude $\hat{B}_a$ by the number of tapes (176) is also plotted. The average power loss (W/m) of an isolated thin strip under alternating magnetic field of amplitude $\hat{B}_a$ in the direction perpendicular to the flat side of the tape is given in (8).

The results can be found in Fig. 4. It can be seen there is good agreement between COMSOL and the modified Clem method. However, simply multiplying the loss of an isolated tape by the number of tapes present in the stack gives results that are much higher than the other two methods. This is due to the shielding effect by other tapes in the stack that is not accounted for if tapes are considered in isolation.

IV. Comparison between individual conductors

Section IV compares the losses of isolated conductors using formulas in Section II.

A. Loss at different current densities

In this Section IV-A, we compare the loss per unit volume of different conductors. The loss per unit volume of a conductor is its loss per unit length divided by the conductor area in

[4]In COMSOL simulations, the E-J power law is used, with $n = 30$, $E_c = 1 \times 10^{-4}$ V/m, $J_c = 2.05 \times 10^{11}$ Am^{-2} of the HTS layer in a tape; HTS layer thickness is 2.35 µm. Magnetic flux density applied perpendicular to the tapes is $\hat{B}_a \sin(2\pi f t) r(t)$ where the ramp function $r(t) = 1/(1+\exp(-5(10ft-1.8)))$, $f = 150$ Hz, and $\hat{B}_a$ is the magnetic flux density amplitude. One period is simulated, and the average magnetization loss is calculated by averaging the loss in the second half of the period simulated.

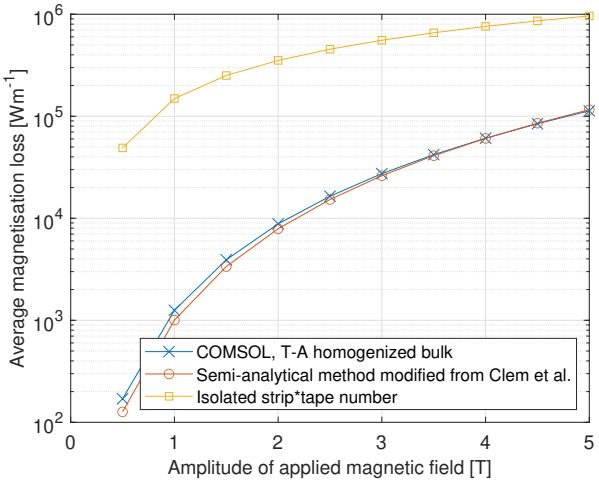

Fig. 4: Magnetization loss of a stack of tapes calculated by the modified Clem method, T-A homogenized method in COMOSL, and the Brandt and Indenbom formula for an isolated strip. Each 4 mm wide tape has $I_c = 1,927$ A. Stack height $2b = 19.64$ mm. Tape separation $D_{\text{sep}} = 111.6$ µm.

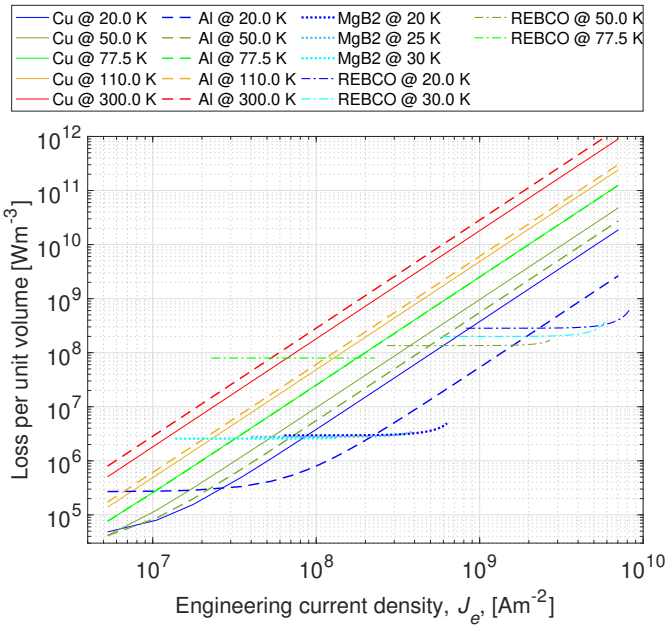

Fig. 5: Loss per unit volume of conductor when an isolated conductor, at different temperatures, is carrying 150 Hz transport ac of different amplitudes (amplitudes converted to engineering current densities) whilst simultaneously being subject to a 150 Hz alternating external magnetic field of amplitude 0.4 T.

Table V. A loss of 1 W/cm^3 = 10^{-6} W/m^3 and is equivalent to a conductor of cross-sectional area of 1 mm^2 generating 1 W of loss per meter in length.

The respective loss per unit volume of conductor when each of the four conductors are transporting ac at different engineering current densities J_e are plotted in Fig. 5, for a few chosen temperatures. The conductors are simultaneously being subject to an alternating external magnetic field of amplitude 0.4 T. The frequency for transport current and magnetic field are both 150 Hz, and this frequency value is assumed throughout Section IV. The J_e is the transport ac amplitude divided by the conductors' cross-sectional areas. The range of transport current evaluated in the plot and the cross-sectional areas of the four conductors are given in Table V. The default REBCO tape used for comparison in Section IV has twist pitch $L_{\text{p,R}} = 0.3$ m [35, Table 1], and has $N_{\text{R}} = 10$ filaments.

From Fig. 5, it can be seen that at 77.5 K, the copper and aluminum Litz wires can achieve lower loss levels than the REBCO tape at J_e less than 1.8 $\times 10^8$ A/m^2, which is 0.79 of the critical engineering current density of the REBCO tape. At 20 K, the aluminum Litz wire offers similar loss as the MgB_2 wire at 2.3×10^8 A/m^2 and as the REBCO tape at 2.3×10^9 A/m^2. However, the MgB_2 wire and REBCO tape still give lower losses at the highest J_e they can achieve, respectively, compared to the aluminum Litz wire.

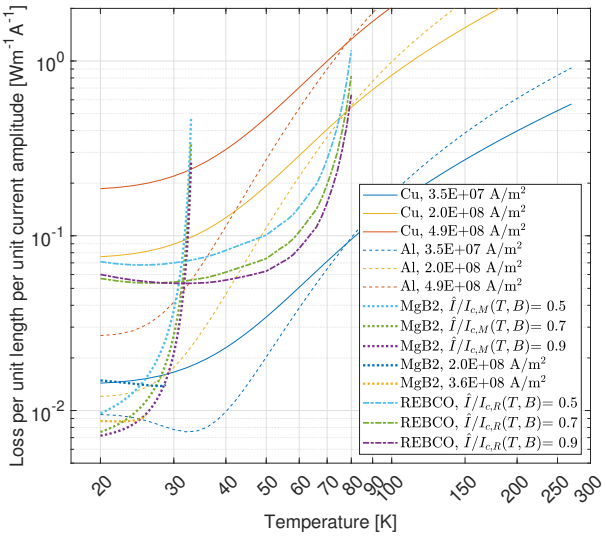

Fig. 6: Loss per unit length of conductor per unit ac amplitude carried when the conductors are carrying the selected transport ac amplitudes at different temperatures. The conductors are simultaneously being subject to an alternating external magnetic field of amplitude 0.4 T. Both the transport ac and the external magnetic field are at 150 Hz.

B. Loss at different temperatures

Next, we plot the loss per unit length per unit current amplitude of the different conductors when they carry different transport ac under different temperatures in Fig. 6. The conductors are simultaneously being subject to an alternating external magnetic field of amplitude 0.4 T. For the copper and aluminum Litz wires, transport current of 100 A, 570 A and 1,400 A are tested and the corresponding J_e are shown in the plot. For the MgB_2 wire and REBCO tape, transport current

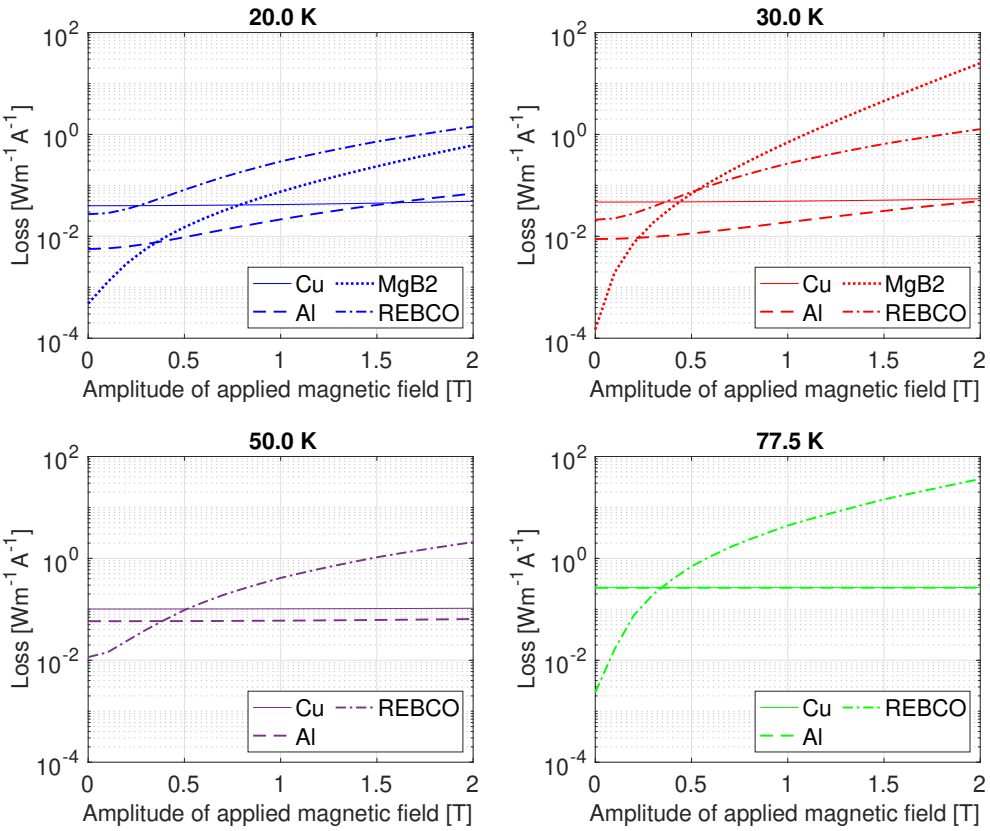

Fig. 7: Loss per unit length of conductor per unit ac amplitude carried when the conductors at different temperatures are subject to alternating external magnetic fields of different amplitudes, whilst carrying transport ac of amplitudes specified in the main text. Both the transport ac and the external magnetic field are at 150 Hz.

TABLE V: Range of Current per Conductor

Conductor	Current range	Conductor area
REBCO tape	0.3 to 0.99 of $I_{c,\mathrm{R}}(T,B)$	$t_{\mathrm{tape}} w_{\mathrm{tape}}$
MgB_2 wire	0.3 to 0.99 of $I_{c,\mathrm{M}}(T,B)$	πr_0^2
Copper Litz wire	15–20,000 A	πr_L^2
Aluminum Litz wire	15–20,000 A	πr_L^2

tested at 50%, 70% and 90% of their respective critical current $I_c(T,B)$ at the different temperatures T, with $B = 0.4$ T.

Whilst carrying higher current (densities) result in higher loss per unit length, Fig. 6 shows that higher current can give lower loss per unit length per unit current for superconductors, so to carry the same current, the overall loss can be lower in superconductors by increasing the current density in the wire than having multiple wires. In contrast, for the Litz wires, the loss is generally higher if the current density is higher. Also, reducing the temperature does not always guarantee lower losses for the aluminum Litz wire and the REBCO tape. This plot is useful when considering which are the best current density and temperature that will generate the lowest loss when carrying the same amount of current.

C. Loss at different magnetic field amplitudes

The loss per unit length per unit current amplitude for the different conductors when they carry a transport ac whilst being subject to alternating external magnetic fields of different amplitudes are plotted in Fig. 7. A few selected temperatures are used. For the copper and aluminum Litz wires, a transport ac amplitude of 300 A is selected; for the MgB_2 wire and the REBCO tape, transport ac amplitudes of 50% and 90%, respectively, of their respective critical currents $I_c(T,B)$ at the B and T shown in Fig. 7 are selected.

Of the temperatures plotted, the loss of the copper and aluminum Litz wires are almost independent of the field except the aluminum Litz wire at 20 K and 30 K. For the superconductors, reducing the field reduces the loss. At fields above 0.7 T at 20 K and above 0.3 T at 77.5 K, the losses of the superconductor(s) are higher than those of the copper and aluminum Litz wires.

V. Comparison between machines made with different conductors

This section considers air-cored radial flux synchronous machines whose armatures are made of the REBCO tape, the MgB_2 wire, the copper Litz wire, and the aluminum Litz wire, respectively. The rotor excitation is not the focus of this paper and it is assumed that for all machine sizes, a magnetic

loading $B_{s0} = 0.4$ T is provided by the rotor excitation. The design of the rotor excitation to provide the same B_{s0} for different machine sizes is outlined in Appendix A. We consider machines with power $P = 3$ MW and speed 4,500 rpm [44]. The frequency f of the field variation and ac supply is taken as 150 Hz, which corresponds to $p = 2$ pole-pairs when the rotation speed is 4,500 rpm. The machine parameters are listed in Table VI. This Section V calculates the armature loss and machine volume when different current densities are carried in the different armature conductors.

A. Sizing of machine

The use of cryogenic normal-state conductors or superconductors can reduce the size of the machine due to their ability to carry high current density. This Section V-A derives a relationship between the current density in the conductor of the armature and the machine volume.

The power of a three-phase generator is [45]

$$P = \frac{\pi^2}{\sqrt{2}} k_w B_{s0} A_s D^2 L n_s, \tag{29}$$

where k_w is the fundamental harmonic winding factor, L is the machine's active length, n_s is the rotational speed (in rev·s^{-1}), A_s is the electric loading [45] $A_s = \frac{6 T_{\text{ph}} I_{\text{rms}}}{\pi D}$, where I_{rms} is the stator phase current (rms), and T_{ph} is the number of turns in series per phase. Adapting A_s to our case where we want to express it in terms of current density of conductor in stator slot area,

$$\begin{aligned} A_s &= \frac{J_{\text{rms,slot}} \times (\text{total stator coil area})}{\pi D} \\ &= \frac{\frac{1}{\sqrt{2}} J \lambda_{\text{fill}} (\pi D \lambda_{\text{cp}}) (\lambda_{\text{ta}} D)}{\pi D} \\ &= \frac{1}{\sqrt{2}} J D \lambda_{\text{fill}} \lambda_{\text{cp}} \lambda_{\text{ta}}, \end{aligned} \tag{30}$$

where we assume the stator winding's radial thickness is $\lambda_{\text{ta}} D$, and λ_{cp} is the fraction of circumference occupied by stator windings, $J_{\text{rms,slot}}$ is the rms of the sinusoidal current density flowing in stator slot area, J is the amplitude of the engineering current density of individual conductors in the stator slots (i.e., the current amplitude carried by the conductor divided by total conductor area of an individual conductor), and λ_{fill} is the fill factor of a stator slot (i.e., proportion of a stator slot's cross-sectional area occupied by conductors).

The interpretations of D and B_{s0} in (29) for air-cored machines are as follows, according to [46]. $D = 2r_a$ where r_a is the mean radius of stator winding, B_{s0} is amplitude of the fundamental of the radial magnetic flux density measured at r_a produced by the rotor field winding. B_{s0} is taken as 0.4 T in this study, and the design of field excitation to produce 0.4 T is outlined in Appendix A.

Let $\alpha = L/D$. Putting (30) in (29), the machine diameter D can be found as a function of current density J in the conductors of the armature,

$$D(J) = \left(\frac{2P}{\pi^2 k_w B_{s0} n_s J \lambda_{\text{ta}} \lambda_{\text{cp}} \lambda_{\text{fill}} \alpha} \right)^{\frac{1}{4}}, \tag{31}$$

TABLE VI: Parameters of Machine

Description	Symbol	Unit	Value
Power	P	W	3×10^6
Rotational speed	n_s	rev·s^{-1}	75
Electrical frequency	f	Hz	150
Number of pole pairs	p	-	2
Fundamental harmonic winding factor	k_w	-	1
Magnetic loading (amplitude of fundamental of the radial component of magnetic flux density at mean armature radius due to rotor excitation)	B_{s0}	T	0.4
Proportion of machine periphery taken by armature winding	λ_{cp}	-	0.5
Radial thickness of armature as a proportion of armature diameter	λ_{ta}	-	0.1
Fill factor of stator slot	λ_{fill}	-	0.5
Ratio of machine length to diameter (L/D)	α	-	0.5

where values of the other parameters are listed in Table VI. The volumes of machine is $\frac{\pi}{4}\alpha D^3$. For ease of reference, the volume of machines for different armature conductor current densities J are plotted in Fig. 8(a), so that the value of J corresponding to different machine volumes can be read off easily.

The validity of (31) is verified in Appendix A, in which machines with different J and corresponding D are designed and their torques are evaluated numerically.

B. Loss of machine armatures with different conductor materials

1) REBCO: This section shows how formulas in Section III can be used to estimate the loss of an REBCO armature in a machine with current density amplitude J in the REBCO tapes, operating at temperature T. In our machine shown in Fig. 9, each slot has radial thickness $w_{\text{slot}} = D\lambda_{\text{ta}}$ and circumferential width $h_{\text{slot}} = \frac{\pi D \lambda_{\text{cp}}}{6p}$. In our calculations of loss, the slots in armature are modified to be rectangular (which is likely to be the case with racetrack REBCO coils). Each slot is thus modeled as a stack of tapes with width w_{stack} equal to w_{slot} rounded to the nearest 4 mm, and height $h_{\text{stack}} = w_{\text{slot}} h_{\text{slot}} / w_{\text{stack}}$. The width of the tapes is w_{stack}. The separation between tapes $D_{\text{sep}} = t_{\text{tape}}/\lambda_{\text{fill}}$.

Each tape carries ac with amplitude $I = J t_{\text{tape}} w_{\text{stack}}$. The critical current I_c of each tape is interpolated from $I_c(T, B)$ data of SuperOx YBCO tape [38] and scaled to width w_{stack}. In particular, the B when performing the interpolation is taken as

$$B = B_{\text{mean}}(J) + B_{\text{s0}}, \tag{32}$$

where $B_{\text{mean}}(J)$ is the mean of magnetic flux density $|\mathbf{B}|$ over the rectangular stack area when current density $J\lambda_{\text{fill}}$ flows uniformly through it. This is a way to take into account the reduced I_c due to self-field when a current flows through the tapes, because J_c is assumed to be constant in formulas in Section III.

Further, the tape turns with minimum current density $I_{\text{c,min}}$ in a stack is found by interpolating $I_c(T, B)$ data with $B =$

$B_{\max}(J) + B_{s0}$, where $B_{\max}(J)$ is the mean $|\mathbf{B}|$ over the area of the rectangular slot where the outermost tapes are located (covering the 5% of stack area) when the rectangular stack area has current density $J\lambda_{\text{fill}}$ flowing uniformly through it. If $I > I_{\text{c,min}}$, the machine with the corresponding J is not evaluated since the current in a tape due to the imposed J will exceed the critical current of the outermost tape turns of the coil.

The transport hysteresis loss (in W/m) of tapes in a slot is estimated as the transport hysteresis loss of a stack (of tapes) with width $2a = w_{\text{stack}}$ and height $2b = h_{\text{stack}}$, which is given by $Q'_{\text{transp}} f$ where Q'_{transp} is from (21). Similarly, the magnetization hysteresis loss (in W/m) of the tapes in a slot is estimated as the magnetization hysteresis loss of a stack of width $2a = w_{\text{stack}}$ and height $2b = h_{\text{stack}}$, which is given by $Q'_{\text{mag}} f$ where Q'_{mag} is from (27). The total loss of REBCO in a machine is the sum of hysteresis and magnetization losses scaled to the length of the machine, multiplied by the number of stator slots.

Note that coupling loss is not considered due to the lack of formulas for the situation of tapes in a stack. Thus, tapes are assumed to be unstriated and of width w_{stack}. The eddy current loss is also not considered because Müller [40, Fig. 3] showed that in an infinitely thick stack ($2b \to \infty$), the eddy current loss when $I/I_c > 0.02$ is at least one order of magnitude smaller than the hysteresis loss when considering transport ac losses. If $I < 0.02 I_c$, the machine is not evaluated to avoid giving inaccurate loss values. Also, when considering magnetization losses, Müller [40, Fig. 7a] showed that if the applied field amplitude $\hat{H}_a = \hat{B}_a/\mu_0$ is such that $\frac{\hat{H}_a}{H_d} > 0.1$, where $H_d = J_{\text{c,HTS}} d/\pi = I_c/(2a\pi)$, d is the thickness of the HTS layer, and $J_{\text{c,HTS}}$ is the critical current density of the HTS layer, then the eddy current loss is at least one order of magnitude less than the hysteresis loss.

Comparison of hysteresis loss in a rectangular slot in a machine calculated numerically in COMSOL and (largely) analytically using the above method can be found in Appendix B.

2) Litz wires and MgB_2: This section calculates the losses of the Litz wires and the MgB_2 wires in the armatures of machines with different engineering current density amplitudes J in the armature conductors. Formulas for isolated wires in Section II will be used, but the external field experienced by each wire will take into account the self-field created by current in other wire turns in the same slot, in addition to the field due to rotor excitation.

For simplicity, the rectangular assumption for the shape of the armature slots will be kept in order to simplify the calculation of magnetic field in different parts of the slot. The rectangular slot has dimensions w_{stack} by h_{stack} (we keep the subscript "stack" for consistency with the previous section on REBCO tape losses). In order to avoid the complexity of evaluating the field experienced by each wire turn in a slot, the rectangular slot is divided into 9 regions with equal areas (a 3-by-3 grid). The mean magnetic flux density amplitude $|\mathbf{B}|$ is found in each of the nine regions (only 4 needs to be evaluated due to symmetry) when current density $J\lambda_{\text{fill}}$ flows uniformly through the rectangular slot area. The loss (in W/m) dissipated by each wire turn in a given region is given by (1a) for a Litz wire and (3) for an MgB_2 wire for a given current amplitude I through the wire and simultaneous application of external ac magnetic field with amplitude B. I is J multiplied by the respective wire cross-sectional areas, and B is

$$B = B_{\text{mean}}(J, \text{region}) + B_{s0} \tag{33}$$

where $B_{\text{mean}}(J, \text{region})$ is the mean $|\mathbf{B}|$ in the region the wire turn is in, $B_{s0} = 0.4$ T is the magnetic loading provided by the rotor excitation. The total number of wire turns in each slot is $w_{\text{stack}} h_{\text{stack}} \lambda_{\text{fill}}/A_{\text{wire}}$ where A_{wire} is the cross-sectional area of the respective MgB_2 or Litz wire. Summing the loss (in W/m) of wire turns in each region of a rectangular slot, and multiplying by the number of armature slots, and multiplying by the length of machine will give the total armature loss for a machine.

When evaluating the loss of an MgB_2 multifilamentary wire in one of the 9 regions of the rectangular slot, the critical current is calculated according to (7a) with external field given by (33). However, we also find the minimum critical current $I_{\text{c,min}}$ of wire turns in the rectangular slot by interpolating $I_c(T, B)$ data with $B = B_{\max}(J) + B_{s0}$, where $B_{\max}(J)$ is the maximum $|\mathbf{B}|$ in the area near the edges of the rectangular slot. If $I > I_{\text{c,min}}$, the machine with the corresponding J is not evaluated since the current in the wire due to the imposed J will exceed the critical current of the outer wire turns of the coil.

The validity of the method proposed to evaluate losses of MgB_2 wires in machine armature is supported by Terao et al. [19]. In [19], the ac loss of MgB_2 multifilamentary wires in a coil carrying transport ac and subject to a rotating magnetic field is calculated using a similar method. The field experienced by the wire turns (which is used in analytical ac loss formulas) is taken as the sum of 1) mean B over slot area due to transport current, and 2) mean B over slot area due to external field. The analytical results agree with well with experiments. In this paper, we have made a slight improvement by dividing the slot area into 9 regions rather than using one mean B for all wires in the slot.

C. Results

Fig. 8(b) plots the volumes and losses of machines when the armatures are made of different conductors at different temperatures carrying ac with different J. The range of J is $10^{6.5} \le J \le 10^{9.5}$, but for MgB_2 and REBCO machines, certain machines within this range of J is not evaluated due to reasons explained in Sections V-B1 and V-B2.

Following a given curve in Fig. 8(b), the smaller the machine volume, the higher the J. At 20 K, at machine volumes below 0.03 m^3 (which corresponds to $J \approx 3 \times 10^7$ A/m^2), armatures with the aluminum Litz wires have the lowest losses, although the losses of REBCO and aluminum Litz wire armatures are similar at machine volume of approximately 0.01 m^3 (corresponding to $J \approx 2 \times 10^8$ A/m^2).

In Fig. 5, which is for isolated conductors, the loss of the MgB_2 wire is higher than that of the aluminum Litz wire below 2×10^8 A/m^2. Thus, it is not too surprising that for machine volumes larger than 0.01 m^3 (corresponding to $J < 2 \times 10^8$

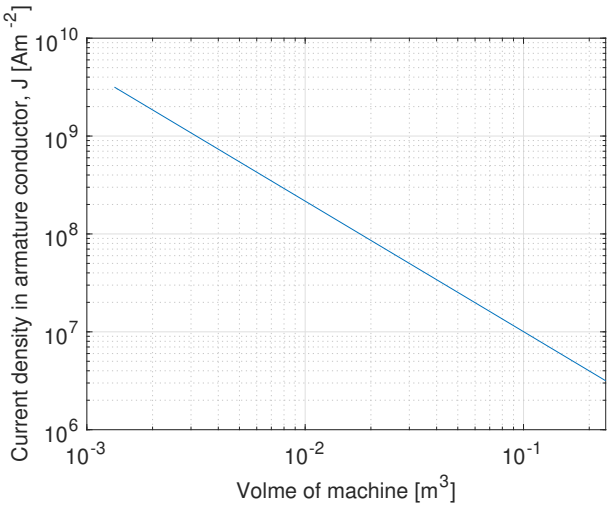

(a)

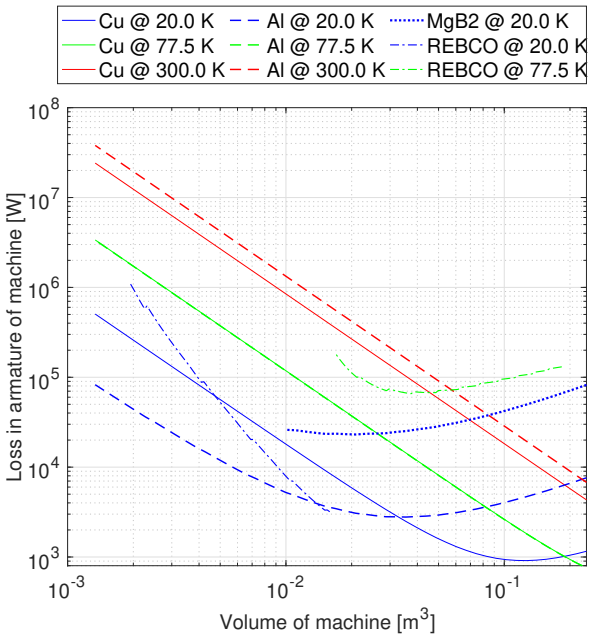

(b)

Fig. 8: (a) The armature conductor engineering current densities that give rise to machines with different volumes. (b) Machine volumes and armature losses of machines whose armatures are made of the different conductors, when the conductors carry ac of different amplitudes at the specified temperatures.

A/m^2), MgB_2 armatures have higher loss. MgB_2 cannot create machines smaller than 0.01 m^3 because at higher J, machines are not evaluated due to reasons explained in Section V-B2.

At 77 K, REBCO armatures have higher losses compared to copper and aluminum Litz wire armatures.

The level of loss permitted in a superconducting motor for aircraft varies in the literature. Berg et al. [47] suggested a target loss of 0.05% or below. In future aircraft, liquid hydrogen on board can function as both fuel and coolant, thus providing free cooling to the machine. Patel et al. [48] estimated the minimum machine efficiency if machine is cooled using only the latent heat of vaporization L of hydrogen, as follows: the power dissipation of the machine generated at operating temperature of superconductor $P_{\text{loss}} = P_{\text{in}}(1-\eta_{\text{m}})$ where η_{m} is the machine's cold efficiency, and P_{in} is the input power to the machine from combustion of hydrogen fuel (either in fuel cell or in gas turbine connected to generator), thus $P_{\text{in}} = \eta_{\text{fc}}\dot{m}_{\text{H2}}H_{\text{c}}$, where H_{c} is the higher heat value of H_2 (142 MJ/kg), and η_{fc} is the efficiency of fuel cell (taken as 0.5 in this paper). If the machine's power loss is to be less than the power needed to vaporize the hydrogen that powers the machine, $P_{\text{loss}} < \dot{m}_{\text{H2}}L$, where L is the latent heat of vaporization of hydrogen (445.6 kJ/kg [49]), then $\eta_m > 1 - \frac{L}{\eta_{\text{c}}H_{\text{c}}} \approx 0.995$. For 3 MW machine, this means loss should be less than 15 kW.

VI. Limitations

This study has the following limitations.

- The coupling loss for a striated REBCO tape depends a lot on the effective transverse resistivity, which is difficult to obtain.
- Different MgB_2 and REBCO have different critical currents and properties depending on manufacturing methods and doping. Here, we select only one set of critical current density for each material.
- The resistivities of copper and aluminum also vary depending on purity. From (2) used in this paper, the resistivity of copper and aluminum at 20 K are 3.60×10^{-10} and 5.07×10^{-11} Ωm, respectively; the resistivity of copper and aluminum at 270 K are 1.54×10^{-8} and 2.48×10^{-8} Ωm, respectively.
- Numerical modelling is required to model conductors under external magnetic field whilst carrying transport current. The analytical formula presented in (3) with the interaction term ignored is just an approximation.
- When considering the loss of machines in REBCO armatures, the width of the tapes is assumed to be the slot thickness in the radial direction rounded to the nearest 4 mm, and the tapes are assumed to be unstriated. This is due to lack of analytical formulas for loss in a finite array of finite stacks of tapes (i.e., stacks of finite height). Using narrower tapes with striation may reduce loss.
- When calculating the volume of machines, geometric constraints have been disregarded, such as lower limit of practical size of machine, e.g., due to minimum winding radius. Although the absolute machine volumes presented may not be practical, the machine volumes relative to each other still provide useful comparison between the conductors.
- The mass of machine is not estimated due to uncertainty in ratio between active and passive mass, and active mass varies depending on whether iron is used and the winding configurations (which affect the end-winding length).
- The loss in the end windings is not considered.

TABLE VII: Summary of Results

Conductor	Cu Litz			Al Litz		MgB_2	REBCO unstriated		REBCO 10 filaments	
Temperature (K)	20	77.5	300	20	77.5	20	20	77.5	20	77.5
Max transport J_e an isolated conductor can carry whilst under external ac field 0.4 T, both at $f = 150$ Hz, such that loss $\leqslant$ certain level										
Max J_e ($\times 10^6$ Am^{-2}): loss $\leqslant 3\times10^6$ W/m^3	89	40	13	230	40	230	–	–	–	–
Max J_e ($\times 10^6$ Am^{-2}): loss $\leqslant 3\times10^8$ W/m^3	890	340	150	2400	350	630[a]	–[d]	240[b]	4600	230[c]
Lowest machine volume such that armature loss $\leqslant$ certain value. $P = 3$ MW, 4,500 rpm, f=150 Hz, $B_{s0} = 0.4$ T										
Min vol ($\times 10^{-3}$ m^3): loss $\leqslant$ 15 kW (i.e., $\eta_m \geqslant 99.5\%$)	11	34	110	4.2	34	–[f]	7.9	–	not tested	not tested

[a] loss 0.050×10^8 W/m^3; [b] loss 0.66×10^8 W/m^3; [c] loss 0.80×10^8 W/m^3

[d] loss below 14.3×10^8 W/m^3 for $J_e < 3500 \times 10^6$ A/m^2; loss $\approx 14.4\times10^8$ W/m^3 at $J_e = 4600 \times 10^6$ A/m^2

[f] min loss approximately 23 kW, volume approximately 20 $\times 10^{-3}$ m^3

VII. Conclusion

The performance of specific copper Litz wire, aluminum Litz wire, MgB_2 multifilamentary wire and REBCO composite tape are compared on an individual conductor level under specific conditions, and on a machine level under specific machine parameters.

On an individual conductor level, for the four conductors (with their specific geometric and electrical properties) under the conditions of alternating external magnetic field of amplitude $\hat{B}= 0.4$ T with transport ac at different amplitudes, both at 150 Hz:

- At 77.5 K, the loss is higher in REBCO than copper and aluminum Litz wires when they carry the engineering current densities below 79% of critical engineering current density of REBCO.
- At 20 K, MgB_2 and aluminum Litz wire carrying 220 MA/m^2 both give the same loss of 3.0 MW/m^3; REBCO and aluminum Litz wire carrying 2,300 M/Am^2 both give the same loss of 220 M/Wm^3. MgB_2 can achieve a maximum of 630 M/Am^2 whilst REBCO can achieve a maximum of 8,200 M/Am^2; and at these current densities, the loss in aluminum Litz wires is higher than the loss in MgB_2 and REBCO, respectively.
- When REBCO tapes carry $0.9I_c(T, B, N_R)$ whilst under external ac magnetic field of amplitude $\hat{B}$: compared to unstriated tapes, striating tapes to 100 filaments can reduce the total loss per unit volume per unit transport current amplitude in $\hat{B}$=0.4 T (by 74% at 77.5 K and 81% at 20 K) and in $\hat{B}$=1 T (by 19% at 77.5 K and 67% at 20 K).

This paper has also considered 3 MW, 4,500 rpm, 2-pole-pair (150 Hz electrical frequency) electrical machines whose armatures are wound with the four conductors, respectively, and whose rotor excitations produce a radial magnetic field with fundamental harmonic of 0.4 T amplitude at mean armature radius. As the armature conductor current density varies:

- At 77.5 K, REBCO is not competitive against copper or aluminum Litz wires, since the Litz wires give lower machine loss at all machine volumes possible by REBCO (machine volume depends on transport current density carried).
- At 20 K, at machine volumes below 0.03 m^3, armatures with aluminum Litz wires have the lowest loss.

Table VII extracts figures of merit from Fig. 5 and 8(b), plus additional simulation for unstriated REBCO, for comparison between conductors.

In conclusion, based on the material properties and analytical formulas from the literature used in this paper, case study results suggest that at 77.5 K, REBCO is not competitive against copper and aluminum Litz wires. At 20 K, on an individual conductor level, for the conditions presented, MgB_2 and REBCO offer lower loss at their respective maximum achievable current densities than aluminum Litz wire. In the machine case study presented, aluminum Litz wire gives the machines with the lowest loss at small machine volumes.

Acknowledgment

The authors would like to thank Prof. Mike Sumption for providing parameters in (7) and Ms. Zhishu Qiu for helpful comments.

Appendix A
Numerical verification of machine sizing equation for air-core machine

This appendix provides sizing formulas to design an air-core machine that outputs the required torque for a 3 MW, 4,500 rpm machine. The general geometry of the machine is given in Fig. 9.

A. Fielding winding design to provide B_{s0}

Consider a sinusoidal sheet current (with unit A/m and is represented as 1D circular line in the 2D model plane) located in air at radius r_f with distribution

$$J_{\text{sheet}} = \hat{J}_{\text{sheet}} \sin(p\theta). \tag{34}$$

By solving Laplace's equation of magnetic vector potential, it can be shown that at radius $r_a > r_f$, the amplitude of the sinusoidal variation of the magnetic flux density in radial direction $B_r(r_a, \theta)$ is [45], [46]

$$B_{s0} = \frac{\mu_0}{2} \hat{J}_{\text{sheet}} \left(\frac{r_f}{r_a}\right)^{p+1}. \tag{35}$$

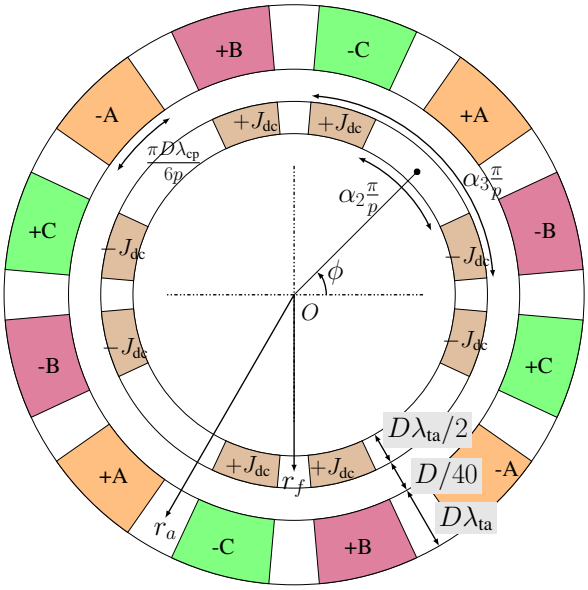

Fig. 9: Topology of the general air-cored machine with $p = 2$ pole pairs. The unit of spans indicated by double-arrow lines in circumferential direction is radians.

In our machine in Fig. 9, the spatial distribution of current density in field excitation coils, when reduced to 1D in the 2D model plane by shrinking the radial direction, can be represented as a sheet current density

$$J_{\text{sheet}} = \sum_{n=1}^{\infty} a_n \sin(np\theta) \tag{36}$$

$$a_n = \frac{4J_{\text{dc}}}{\pi n}\left(\cos\left(\frac{n\alpha_2\pi}{2}\right) - \cos\left(\frac{n\alpha_3\pi}{2}\right)\right) d_f, \tag{37}$$

where $d_f = D\lambda_{\text{ta}}/2 = r_a\lambda_{\text{ta}}$ is the radial thickness of field coils, and we assume rotor is at position $\phi = 0$.

At radius $r_a > r_f$, it can be shown that

$$B_r(r_a,\theta) = \sum_{n=1}^{\infty} \frac{\mu_0}{2}\left(\frac{r_f}{r_a}\right)^{np+1} a_n \cos(np\theta). \tag{38}$$

The fundamental component of $B_r(r_a,\theta)$ has amplitude,

$$\begin{aligned} B_{s0} &= \frac{\mu_0}{2}\left(\frac{r_f}{r_a}\right)^{p+1} a_1 \\ &= \left(\frac{r_f}{r_a}\right)^{p+1} \frac{2\mu_0 J_{\text{dc}} d_f}{\pi}\left(\cos\left(\frac{\alpha_2\pi}{2}\right) - \cos\left(\frac{\alpha_3\pi}{2}\right)\right). \end{aligned} \tag{39}$$

So to design a rotor field excitation that creates $B_{s0} = 0.4$ T at $r = r_a = D/2$, when D varies, J_{dc} has to be set as

$$J_{\text{dc}} = \frac{B_{s0}\pi}{2\mu_0\left(\frac{r_f}{r_a}\right)^{p+1} d_f\left(\cos\left(\frac{\alpha_2\pi}{2}\right) - \cos\left(\frac{\alpha_3\pi}{2}\right)\right)}. \tag{40}$$

For simplicity, we set $\alpha_2 = 0.5, \alpha_3 = 0.75, d_f = D\lambda_{\text{ta}}/2$, and airgap (radial distance between inner stator coil radius and outer rotor coil radius) to be $D/40$.

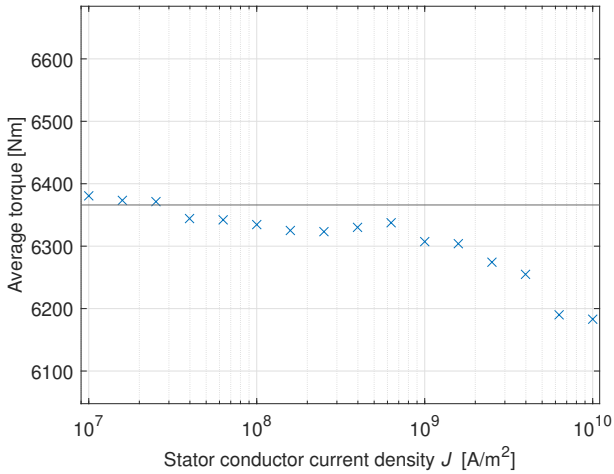

Fig. 10: Average torque of machines with different J. The range of the y axis is 5% of the desired torque 6,366 Nm (plotted as the black line).

B. *Verification of sizing equation*

From (31), D is a function of the conductor's engineering current density amplitude J, and we vary J to get machines with different D in Fig. 8(a) and 8(b). To verify the validity of (31), i.e., that machines with the J-D relationship in (31) can indeed output a power of 3 MW at 4,500 rpm (corresponding to a torque of 6,366 Nm), we design different machines by varying J and using (31) to set D and using (40) to design the field excitation to give $B_{s0} = 0.4$ T. Indeed, the machine geometry is automatically set given J. The torque output by the machines as they rotate are evaluated in COMSOL, and the average torque[5] by machines with different J are plotted in Fig. 10. The average torque output is within 3% of the required torque of 6,366 Nm for machines with different J.

As a specific example, for the machine with $J = 10^9$ A/m^2, $D = 0.201$ m according to (31) and J_{dc} according to (40), the B_r at $r_a = D/2$ due to rotor excitation alone is plotted in Fig. 11, which verifies that the field excitation produces a B_r with fundamental component amplitude of 0.4 T at $r = r_a$. The torque generated as the rotor rotates is plotted in Fig. 12, giving an average torque of 6,307 Nm, which is acceptable.

APPENDIX B
NUMERICAL SIMULATION OF AC LOSS OF REBCO ARMATURE

This appendix simulates two machines with $J = 2 \times 10^9$ A/m^2 and $J = 1.3 \times 10^8$ A/m^2 in the REBCO tapes in the armatures. These J values are close to the corresponding machines at the end points of the line for 20 K REBCO in Fig. 8(b). The COMSOL simulation loss results are compared to transport and magnetization loss results calculated by the

[5]One electrical period $(1/f)$ is simulated, and the average torque is calculated over the second half of the period, since the armature and field current densities are multiplied by a ramp function $r(t) = 1/(1+\exp(-5(10ft-1.8)))$ to ensure zero initial conditions for ease of simulation.

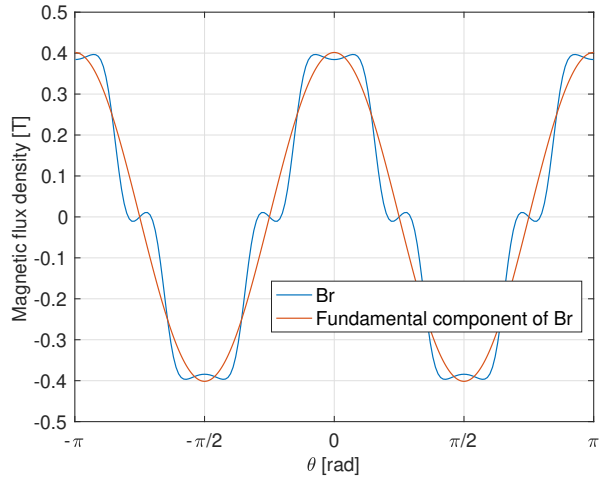

Fig. 11: B_r at $r = r_a = D/2$ for the machine with $J = 10^9$ A/m^2. The fundamental component B_{s0} is 0.4 T, as expected.

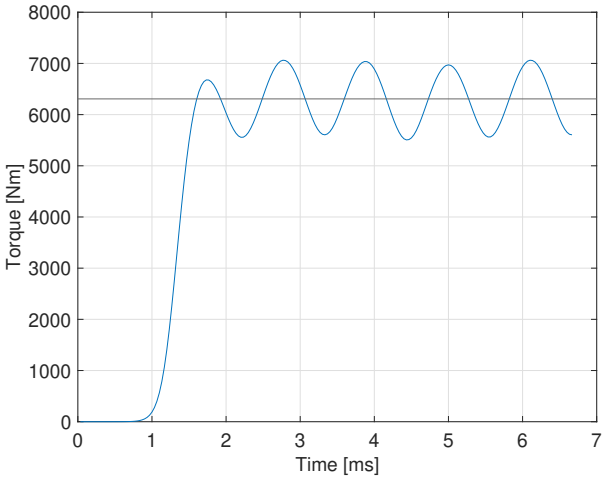

Fig. 12: Torque generated by the machine with $J = 10^9$ A/m^2. The torque is calculated by Arkkio torque in COMSOL. The average torque generated by this machine (6,307 Nm) is also plotted.

semi-analytical methods in Sections III-A and III-B, respectively.

In COMSOL simulations, the armature coils are rectangles as described in Section V-B1. All slots except one have spatially uniform current density, and current distribution in REBCO tapes is modeled for one slot. There are two COMSOL simulations for each machine. In the first simulation, the REBCO tapes in the slot is modeled as a one stack (thus one bulk) using the T-A homogenized formulation. Thus, the tapes are assumed to be as wide as the stack width w_{stack}, as stated in V-B1. In the other simulation, since w_{stack} are in multiples of 4 mm, the tapes are modeled as multiple stacks, each stack with width 4 mm, and the stack height remains unchanged. The stacks are separated by 0.1 mm. This second geometry can be modeled in COMSOL but we have not encountered

TABLE VIII: Loss of REBCO in an Armature Slot in a Machine Environment

Description	Case 1	Case 2
Modeled as one stack		
Amplitude of engineering current density of tape J [A/m^2]	2×10^9	1.3×10^8
Stack width $w_{\text{stack}} = 2a$ [mm]	16	32
Stack height $h_{\text{stack}} = 2b$ [mm]	23.3	45.7
Tape separation D_{sep} [mm]	0.111	0.111
Critical current of a tape I_c [A]	519×4	$1,240 \times 8$
Transport current amplitude per tape I [A]	445×4	28.9×8
Amplitude of external field[1] $\hat{B}$ [T]	0.4	0.4
Transport loss by Clem method [9] [W/m]	1.23×10^6	1,280
Magnetization loss by modified Clem method [W/m]	571	475
Total loss calculated by COMSOL[2] [W/m]	921,000	6,830
Modeled as multiple stacks		
Stack width $w_{\text{stack}} = 2a$ [mm]	4	4
Stack height $h_{\text{stack}} = 2b$ [mm]	23.3	45.7
Number of stacks	4	8
Tape separation D_{sep} [mm]	0.111	0.111
Critical current of a tape I_c [A]	519	1,240
Transport current amplitude per tape I [A]	445	28.9
Total loss calculated by COMSOL[2] [W/m]	824,000	26,200

[1] For calculation of magnetization loss by the modified Clem method. Amplitude of external field is taken as the magnetic loading B_{s0}. In COMSOL, the stack(s) are in a machine environment under a rotating external magnetic field.
[2] Averaged over the second half of the electrical period simulated. Note for Case 2, when the slot is modeled as one stack, we simulate 1.5 electrical period and the average over the last half period is slightly higher, at 6,990 W/m.

analytical formulas to model a finite array of finite stacks.

The results are shown in Table VIII. For the one-stack model in Case 1 ($J = 2 \times 10^9$ A/m^2), there is reasonable agreement between the semi-analytical and numerical (COMSOL) results. The difference is larger for Case 2 ($J = 1.3 \times 10^8$ A/m^2) when the transport current is only 2.3% of the tapes' I_c. The discrepancy between numerical and semi-analytical methods is due to many factors, e.g., the transport ac loss and magnetization loss are calculated separately in semi-analytical methods, but they interact and COMSOL calculates the total loss; the actual stack is subject to rotating magnetic field but we assume the field is in the stack height direction and uniform in space when calculating the magnetization loss using the semi-analytical method. When separating the stack into narrower stacks, COMSOL results show a reduced loss in Case 1 and an increased loss in Case 2. The reasons for such behavior is subject to further investigation.

REFERENCES

[1] GKN Aerospace. (2022) GKN aerospace's cryogenic hyperconducting technology unlocks hydrogen electric propulsion for large aircraft. Accessed: Feb. 17, 2024. [Online]. Available: https://www.gknaerospace.com/en/newsroom/news-releases/2022/gkn-aerospaces-cryogenic-hyperconducting-technology-unlocks-hydrogen-electric-propulsion-for-large-aircraft/

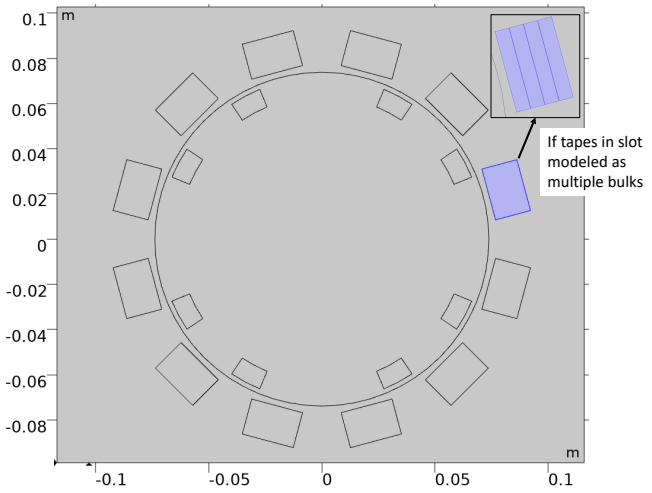

Fig. 13: The machine geometry modeled in COMSOL for the case $J = 2$ GA/m^2. The highlighted slot is modeled as a homogenized bulk via the homogenized T-A formulation (the main figure shows the model when the slot has one stack of tapes only), other slot areas are modeled to have time-varying but spatially uniform current densities. The inset shows the model when the slot has multiple homogenized stacks.

[2] F. Grilli *et al.*, "Superconducting motors for aircraft propulsion: The Advanced Superconducting Motor Experimental Demonstrator project," *J. Phys.: Conf. Ser.*, vol. 1590, 2020, Art. no. 012051.

[3] L. Ybanez *et al.*, "ASCEND: The first step towards cryogenic electric propulsion," *IOP Conf. Ser.: Mater. Sci. Eng.*, vol. 1241, 2022, Art. no. 012034.

[4] M. D. Sumption, "AC loss of superconducting materials in motors and generators for very high density motors and generators for hybrid-electric aircraft," in *Proc. 2018 AIAA/IEEE Electric Aircraft Technol. Symp.*, Cincinnati, OH, USA, Jul. 9–11 2018.

[5] M. D. Sumption, J. Murphy, M. Susner, and T. Haugan, "Performance metrics of electrical conductors for aerospace cryogenic motors, generators, and transmission cables," *Cryogenics*, vol. 111, 2020, Art. no. 103171.

[6] T. J. Haugan, M. A. P. Sebastian, C. J. Kovacs, M. D. Sumption, and B.-H. Tsao, "Design and scaling laws of a 40-MW-class electric power distribution system for liquid-H_2 fuel-cell propulsion," in *Proc. AIAA Propulsion Energy 2021 Forum*, Virtual event, Aug. 9–11 2021.

[7] S. S. Kalsi, R. Badcock, J. Storey, K. A. Hamilton, and Z. Jiang, "Motors employing REBCO CORC and MgB_2 superconductors for ac stator windings," *IEEE Trans. Appl. Supercond.*, vol. 31, no. 9, 2021, Art. no. 5206807.

[8] G.-D. Nam, H.-J. Sung, B.-S. Go, M. Park, and I.-K. Yu, "Design and comparative analysis of MgB_2 and YBCO wire-based-superconducting wind power generators," *IEEE Trans. Appl. Supercond.*, vol. 28, no. 3, 2018, Art. no. 5205605.

[9] J. R. Clem, J. H. Claassen, and Y. Mawatari, "AC losses in a finite Z stack using an anisotropic homogeneous-medium approximation," *Supercond. Sci. Technol.*, vol. 20, no. 12, pp. 1130–1139, 2007.

[10] W. Yuan, A. M. Campbell, and T. A. Coombs, "A model for calculating the ac losses of second-generation high temperature superconductor pancake coils," *Supercond. Sci. Technol.*, vol. 22, no. 7, 2009, Art. no. 075028.

[11] C. D. Manolopoulos, M. F. Iacchetti, A. C. Smith, P. Miller, and M. Husband, "Litz wire loss performance and optimization for cryogenic windings," *IET Electric Power Appl.*, vol. 17, no. 4, pp. 487–498, 2023.

[12] Elektrisola. (2024) Technical data by dimensions. Accessed: 6 October 2024. [Online]. Available: https://www.elektrisola.com/en/Products/Litz-Wire/Dimensions

[13] A. Woodworth *et al.*, "Thermal analysis of potted Litz wire for high power density aerospace electric machines," in *Proc. AIAA Propulsion Energy 2019 Forum*, Indianapolis, IN, USA, Aug. 19–22 2019.

[14] J. Martin, A. Yoon, A. Jin, and K. S. Haran, "High-frequency Litz "air-gap" windings for high-power density electrical machines," *Electric Power Components Syst.*, vol. 45, no. 7, pp. 798–805, 2017.

[15] X. Yi, T. Yang, J. Xiao, N. Miljkovic, W. P. King, and K. S. Haran, "Equivalent thermal conductivity prediction of form-wound windings with Litz wire including transposition effects," *IEEE Trans. Ind. Appl.*, vol. 57, no. 2, pp. 1440–1449, 2021.

[16] M. D. Sumption, "AC loss of superconducting materials-refined loss estimates of MgB_2 wires for superconducting motors and generators," in *Proc. AIAA Propulsion Energy 2019 Forum*, Indianapolis, IN, USA, Aug. 19–22 2019.

[17] T. Balachandran, D. Lee, N. Salk, and K. S. Haran, "A fully superconducting air-core machine for aircraft propulsion," *IOP Conf. Ser.: Mater. Sci. Eng.*, vol. 756, no. 1, 2020, Art. no. 012030.

[18] Y. Terao, W. Kong, H. Ohsaki, H. Oyori, and N. Morioka, "Electromagnetic design of superconducting synchronous motors for electric aircraft propulsion," *IEEE Trans. Appl. Supercond.*, vol. 28, no. 4, 2018, Art. no. 5208005.

[19] Y. Terao, H. Nakamura, S. Okumura, S. Fuchino, and H. Ohsaki, "AC loss of MgB_2 superconducting coils with alternating transport current in rotating magnetic field," *IEEE Trans. Appl. Supercond.*, vol. 33, no. 5, 2023, Art. no. 3600305.

[20] W. J. Carr Jr., *AC Loss and Macroscopic Theory of Superconductors*, 2nd ed. USA and Canada: Taylor & Francis Inc., 2001.

[21] C. Zhou, "Intra wire resistance and strain affecting the transport properties of Nb_3Sn strands in cable-in-conduit conductors," Ph.D. dissertation, University of Twente, The Netherlands, 2014.

[22] T. Garg *et al.*, "Development and testing of a three-period, subsize 2G AIMI MgB_2 planar undulator," *Supercond. Sci. Technol.*, vol. 37, no. 1, 2024, Art. no. 015011.

[23] A. Godfrin *et al.*, "Influence of the striation process and the thickness of the Cu-stabilization on the ac magnetization loss of striated REBCO tape," *IEEE Trans. Appl. Supercond.*, vol. 27, no. 6, 2017, Art. no. 5900809.

[24] A. Molodyk *et al.*, "Development and large volume production of extremely high current density $YBa_2Cu_3O_7$ superconducting wires for fusion," *Sci. Rep.*, vol. 11, no. 1, 2021, Art. no. 2084.

[25] J. Lu, E. S. Choi, and H. D. Zhou, "Physical properties of hastelloy® C-276™ at cryogenic temperatures," *J. Appl. Phys.*, vol. 103, 2008, Art. no. 064908.

[26] R. A. Matula, "Electrical resistivity of copper, gold, palladium, and silver," *J. Phys. Chem. Ref. Data*, vol. 8, no. 4, pp. 1147–1298, 1979.

[27] A. C. C. Wulff, A. B. Abrahamsen, and A. Insinga, "Topical review: Multifilamentary coated conductors for ultra-high magnetic field applications," *Supercond. Sci. Technol.*, vol. 34, 2021, Art. no. 053003.

[28] F. Grilli and A. Kario, "How filaments can reduce ac losses in HTS coated conductors: A review," *Supercond. Sci. Technol.*, vol. 29, no. 8, 2016, Art. no. 083002.

[29] E. H. Brandt and M. Indenbom, "Type-II-superconductor strip with current in a perpendicular magnetic field," *Phys. Rev. B Condens Matter*, vol. 48, no. 17, pp. 12 893–12 906, 1993. [Online]. Available: https://www.ncbi.nlm.nih.gov/pubmed/10007663

[30] Y. Mawatari, "Critical state of periodically arranged superconducting-strip lines in perpendicular fields," *Phys. Rev. B Condens Matter*, vol. 54, no. 18, pp. 13 215–13 221, 1996.

[31] W. J. Carr Jr., "Sheath and substrate losses in high-Tc superconductors," *Adv. Cryogenic Eng. Mater.*, vol. 44B, pp. 593–600, 1998.

[32] K.-H. Müller, "AC power losses in flexible thick-film superconducting tapes," *Physica C*, vol. 281, p. 1–10, 1997.

[33] R. Gyuraki *et al.*, "Interfilament resistance at 77 K in striated HTS coated conductors," *IEEE Trans. Appl. Supercond.*, vol. 26, no. 8, 2016, Art. no. 6603606.

[34] E. Demencik *et al.*, "AC loss and coupling currents in YBCO coated conductors with varying number of filaments," *IEEE Trans. Appl. Supercond.*, vol. 24, no. 6, 2014, Art. no. 6601008.

[35] C. E. Oberly, L. Long, G. L. Rhoads, and W. J. Carr Jr., "AC loss analysis for superconducting generator armatures wound with subdivided Y–Ba–Cu–O coated tape," *Cryogenics*, vol. 41, pp. 117–124, 2001.

[36] W. J. Carr and C. E. Oberly, "Transverse resistivity of a filamentary coated conductor," *Supercond. Sci. Technol.*, vol. 19, no. 1, pp. 64–67, 2006.

[37] N. Amemiya *et al.*, "AC loss reduction of YBCO coated conductors by multifilamentary structure," *Supercond. Sci. Technol.*, vol. 17, no. 12, pp. 1464–1471, 2004.

[38] S. Wimbush, N. Strickland, and A. Pantoja. (2021) Critical current characterisation of SuperOx YBCO 2G HTS superconducting wire. [Online]. Available: https://doi.org/10.6084/m9.figshare.13708690.v1

[39] K.-H. Müller, "Self-field hysteresis loss in periodically arranged superconducting strips," *Phys. C: Supercond.*, vol. 289, no. 1-2, pp. 123–130, 1997.
[40] ——, "AC losses in stacks and arrays of YBCO/hastelloy and monofilamentary Bi-2223/Ag tapes," *Phys. C: Supercond.*, vol. 321, no. 1-2, pp. 149–167, 1999.
[41] G. P. Mikitik, Y. Mawatari, A. T. S. Wan, and F. Sirois, "Analytical methods and formulas for modeling high temperature superconductors," *IEEE Trans. Appl. Supercond.*, vol. 23, no. 2, 2013, Art. no. 8001920.
[42] E. Berrospe-Juarez, V. M. R. Zermeño, F. Trillaud, and F. Grilli, "Real-time simulation of large-scale HTS systems: multi-scale and homogeneous models using the T–A formulation," *Supercond. Sci. Technol.*, vol. 32, no. 6, 2019, Art. no. 065003.
[43] W. T. Norris, "Calculation of hysteresis losses in hard superconductors carrying ac: Isolated conductors and edges of thin sheets," vol. 3, no. 4, p. 489–507, 1970.
[44] J. L. Felder, G. V. Brown, H. D. Kim, and J. Chu, "Turboelectric distributed propulsion in a hybrid wing body aircraft," in *Proc. 20th Int. Soc. Airbreathing Engines (ISABE 2011)*, Gothenburg, Sweden, Sep. 12–16 2011. [Online]. Available: https://ntrs.nasa.gov/citations/20120000856
[45] T. J. E. Miller and A. Hughes, "Comparative design and performance analysis of air-cored and iron-cored synchronous machines," *Proc. Inst. Electr. Eng.*, vol. 124, no. 2, pp. 127–132, 1977.
[46] G. Galantini, "Preliminary design and simulation of a superconducting synchronous machine for aircraft applications," Master's thesis, Politecnico di Torino, Italy, 2022.
[47] F. Berg, J. Palmer, P. Miller, and G. Dodds, "HTS system and component targets for a distributed aircraft propulsion system," *IEEE Trans. Appl. Supercond.*, vol. 27, no. 4, 2017, Art. no. 3600307.
[48] A. Patel, V. Climente-Alarcon, A. Baskys, B. A. Glowacki, and T. Reis, "Design considerations for fully superconducting synchronous motors aimed at future electric aircraft," in *Proc. 2018 IEEE Int. Conf. Elect. Syst. Aircraft, Railway, Ship Propulsion Road Veh. & Int. Transp. Electrific. Conf. (ESARS-ITEC)*, Nottingham, UK, Nov. 7–9 2018.
[49] R. Radenbaugh, "Refrigeration for superconductors," *Proc. IEEE*, vol. 92, no. 10, pp. 1719–1734, 2004.